APPLIED SCIENCES AND ENGINEERING

Robot-assisted chirality-tunable acoustic vortex tweezers for contactless, multifunctional, 4-DOF object manipulation

Teng Li[1], Jiali Li[1], Luyu Bo[1], Hunter Bachman[2], Bei Fan[3]*, Jiangtao Cheng[1]*, Zhenhua Tian[1]*

Robotic manipulation of small objects has shown great potential for engineering, biology, and chemistry research. However, existing robotic platforms have difficulty in achieving contactless, high-resolution, 4-degrees-of-freedom (4-DOF) manipulation of small objects, and noninvasive maneuvering of objects in regions shielded by tissue and bone barriers. Here, we present chirality-tunable acoustic vortex tweezers that can tune acoustic vortex chirality, transmit through biological barriers, trap single micro- to millimeter-sized objects, and control object rotation. Assisted by programmable robots, our acoustic systems further enable contactless, high-resolution translation of single objects. Our systems were demonstrated by tuning acoustic vortex chirality, controlling object rotation, and translating objects along arbitrary-shaped paths. Moreover, we used our systems to trap single objects in regions with tissue and skull barriers and translate an object inside a Y-shaped channel of a thick biomimetic phantom. In addition, we showed the function of ultrasound imaging–assisted acoustic manipulation by monitoring acoustic object manipulation via live ultrasound imaging.

INTRODUCTION

Precision contactless object manipulation has shown great potential for engineering, biology, and chemistry research, such as controlling microrobots, handling delicate bioparticles (e.g., exosomes and cells), transporting hazardous reagent droplets, controlling self-assembly of colloidal materials, and arranging nanomaterials for composite fabrication (*1*–*6*). Among various contactless manipulation methods—such as optical (*2*, *7*), electrical (*3*, *8*), magnetic (*4*, *9*), and acoustic techniques (*10*–*21*)—acoustic tweezers have been attracting increasing attention in recent years. While other methods rely on an object's optical, electrical, or magnetic properties, the success of acoustic tweezers highly depends on the object's compressibility and acoustic impedance (*22*–*24*). Moreover, acoustic tweezers offer multiple appealing features including biocompatibility, the ability to penetrate barriers (e.g., tissue, glass, petri dish, etc.), and the ability to manipulate a variety of objects with different sizes and material properties (e.g., soft, hard, gaseous, and liquid samples) (*22*–*25*). With these features, acoustic tweezers have been successfully applied to manipulate nanometer-sized exosomes (*26*, *27*), micrometer-sized cells (*28*–*34*), and millimeter-sized zebrafish larvae (*35*, *36*), and they have shown great potential for a wide range of applications, including isolating extracellular vesicles for disease diagnosis (*26*, *27*), isolating tumor cells (*37*–*39*), controlling cell-cell interaction (*28*, *40*), arranging cells for bioprinting (*29*–*33*), concentrating biomarkers for signal enhancement (*41*–*43*), driving microrobots (*44*–*47*), and arranging micro/nanofillers for composite fabrication (*48*–*52*).

The increasing array of acoustic object manipulation applications has been enabled by advances in acoustic device mechanisms. Leveraging standing acoustic waves generated from 1 or 2 pairs of transducers, researchers could arrange randomly distributed objects into parallel line–like or rectangular grid–like periodic patterns, separate objects with different sizes, and control cell-cell distances (*28*, *53*–*56*). Improving upon this performance, mechanisms based on acoustic arrays with more transducer pairs were developed to better control acoustic interference and arrange particles into more periodic patterns (*57*–*59*). Recently, the acoustic holography mechanism has been introduced to construct even more complex particle patterns (e.g., patterns depicting letters) based on the transformation of incident acoustic fields to desired patterns using three-dimensional (3D) printed or microfabricated holographic lenses (*13*, *60*, *61*). Very recently, holographic transducers with Archimedes spiral-shaped electrodes on flat piezoelectric wafers have been developed to generate a focalized acoustic vortex to enable selective trapping and 2D translation of single microparticles (*62*, *63*).

Despite tremendous progress in acoustic object manipulation mechanisms, existing technology still has several grand challenges that need to be addressed. First, no platforms can achieve contactless 4-degrees-of-freedom (4-DOF) manipulation (including 3D translation u_x, u_y, and u_z and rotation Ω_z) of different-sized (e.g., micro- to millimeter-sized) single objects with high resolution in a large 3D space (e.g., 10 cm by 10 cm by 10 cm). This ability is desired for 3D positioning of biological samples (e.g., cells, spheroids, embryos, and zebrafish larvae) and observing those samples from different directions by rotating them. The 4-DOF manipulation capability also has great potential for the bottom-up assembly of small objects with the orientation and location of each object being well controlled. Second, most acoustic tweezers platforms have difficulty transmitting sufficient acoustic energy through biological barriers (e.g., tissue and bone) to create so-called "through-biological-barrier" acoustic tweezers for shielded object manipulation. Although recent studies have shown in vivo acoustic manipulation of microparticles within a zebrafish (*36*) and bacteria within the near-surface blood vessels of a mouse (*21*), the tissue barriers are very thin, and the manipulated targets are close (e.g., <5 mm) to the acoustic transducers. In particular, no studies have successfully demonstrated acoustic manipulation of

[1]Department of Mechanical Engineering, Virginia Polytechnic Institute and State University, Blacksburg, VA 24060, USA. [2]Department of Mechanical Engineering and Engineering Sciences, University of North Carolina at Charlotte, Charlotte, NC 28223, USA. [3]Department of Mechanical Engineering, Michigan State University, East Lansing, MI 48824, USA.
*Corresponding author. Email: fanbei1@msu.edu (B.F.); chengjt@vt.edu (J.C.); tianz@vt.edu (Z.T.)

objects in the 3D space surrounded by a real skull. Third, acoustic tweezing platforms traditionally use optical cameras to monitor the object manipulation process, limiting their use to optically transparent media; very few studies consider the fusion of ultrasound imaging with acoustic tweezers, although this combination is highly desirable due to its ability to monitor the acoustic object manipulation process in nontransparent media.

This paper presents robot-assisted chirality-tunable acoustic vortex tweezers (illustrated in Fig. 1), which leverage a unique chirality-tunable acoustic vortex tweezing device integrated with a programmable robot, for enabling contactless, multifunctional, high-resolution, 4-DOF manipulation of micro- to millimeter-sized single objects in a large 3D space. Moreover, our acoustic device can generate through-biological-barrier acoustic vortex tweezers to trap and manipulate objects in the 3D space shielded by biological barriers (e.g., tissue and skull) and can be integrated with ultrasound phased array imaging for monitoring the acoustic object manipulation process. To enable these abilities, we developed a chirality-tunable acoustic vortex tweezing device that uses a coaxial holographic chiral acoustic lens to transform coaxial incident acoustic waves into counter-chirality–focused acoustic vortex beams (see Fig. 2B). Compared to previous hologram-based acoustic devices, our device is able to switch acoustic vortex chirality and tune the acoustic orbital angular momentum by modulating a dual-frequency excitation signal. Hence, our device can generate acoustic tweezers to not only trap an object at the center of the vortex beam's ring-shaped potential field but also control the rotation (Ω_z) of the trapped object. With the assistance of programmable robotic modules, our acoustic platform further enables high-resolution 3D translation (u_x, u_y, and u_z) of the acoustically trapped micro- to millimeter-sized single objects in a large 3D space. To demonstrate the capabilities of the robot-assisted chirality-tunable acoustic vortex tweezers, a series of experiments were performed showing the trapping of micro- to millimeter-sized single objects, the control of an object's rotation, as well as the translation of single objects along 2D letter-like and 3D helical paths. We also demonstrated through-biological-barrier acoustic vortex tweezers by transmitting acoustic vortex beams through a ~6-mm-thick tissue with the skin and a ~1.6-mm-thick skull to trap and rotate single objects and translating an object inside a Y-shaped channel in a 36-mm-thick synthetic gelatin phantom, mimicking a tissue with a branched blood vessel. Last, the acoustic tweezing system was combined with ultrasound imaging to monitor the translation of an acoustically trapped object along a complex letter-like path. The functionalities demonstrated by our developed platform prove its huge potential in a wide range of applications ranging from advanced manufacturing to clinical medicine.

RESULTS

Robot-assisted chirality-tunable acoustic vortex tweezers

The robot-assisted chirality-tunable acoustic vortex tweezing system (see Fig. 1 and fig. S1 for schematics and photos) has two key modules: an acoustic device that can generate chirality-tunable acoustic vortex tweezers to trap and rotate single objects and a programmable robotic module to translate and tilt the acoustic device together with the trapped single objects in a large 3D space. Particularly, the chirality-tunable acoustic vortex tweezing device (see Fig. 2A and fig. S1C for a schematic and a photo) takes advantage of coaxial ring transducers to generate coaxial incident waves at different frequencies, a coaxial holographic chiral acoustic lens for transforming different-frequency coaxial incident waves to focused acoustic vortex beams with different chiralities, and a frequency multiplexing–based device control mechanism. As illustrated in Fig. 2A, the coaxial holographic chiral acoustic lens is spatially divided into inner and outer regions (with radius $r_c \le r < r_{in}$ and $r_{in} \le r \le r_{out}$) that have spatially varying thickness profiles $h_{in}(\mathbf{x})$ and $h_{out}(\mathbf{x})$, respectively. The inner and outer coaxial ring transducers (with radius $r_c \le r < r_{in}$ and $r_{in} \le r \le r_{out}$) can generate z-propagation incident waves at angular frequencies of ω_H and ω_L, respectively. As different frequency coaxial incident waves transmit through the lens' inner and outer regions, they are transformed into waves with spatially varying phase profiles, resulting from the acoustic lens-induced position-dependent phase shifts given by

$$\begin{cases} \varphi_{in}(\mathbf{x}) = [k_f(\omega_H) - k_{lens}(\omega_H)]h_{in}(\mathbf{x}) & \text{when } r_c \le |\mathbf{x}| < r_{in} \\ \varphi_{out}(\mathbf{x}) = [k_f(\omega_L) - k_{lens}(\omega_L)]h_{out}(\mathbf{x}) & \text{when } r_{in} \le |\mathbf{x}| \le r_{out} \end{cases} \quad (1)$$

where k_{lens} and k_f are wavenumbers of acoustic waves in the lens and the surrounding medium, respectively. By carefully designing the acoustic lens' thickness profile, we can apply any desired position-dependent phase shifts to incident acoustic waves and further transform the incident waves into desired acoustic beams. The thickness profile $h_{in}(\mathbf{x})$ of the lens inner section is carefully designed to transform an incident wave at a high frequency of ω_H to a confined vortex beam with a topological charge number of $+Q$. On the other hand,

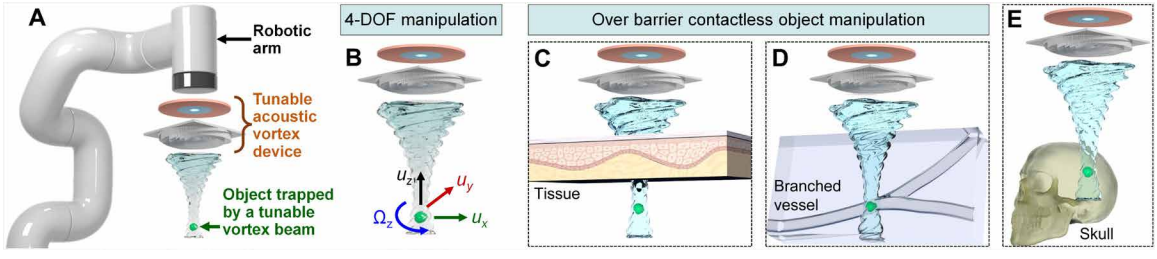

Fig. 1. Illustrations of robot-assisted chirality-tunable acoustic vortex tweezers for contactless, multifunctional, 4-DOF object manipulation. (**A**) Schematic of a robot-assisted acoustic vortex tweezing system that has a chirality-tunable acoustic vortex tweezing device integrated with a robotic arm. (**B**) Illustration of 4-DOF object manipulation. The acoustic vortex device can generate a chirality-tunable acoustic vortex beam to trap an object at the vortex center and control the object rotation Ω_z. The integrated robotic system can achieve 3D translation (u_x, u_y, and u_z) of the acoustically trapped object in a contactless, high-precision, and programmable manner. With these features, the robot-assisted acoustic vortex tweezing system offers shielded object manipulation functionality such as (**C**) penetrating a thick tissue to trap and manipulate an object on the other side of the tissue, (**D**) generating contactless acoustic tweezers in a complex blood vessel to trap and translate an object in the blood vessel, and (**E**) penetrating a skull to trap and manipulate an object in the space surrounded by the skull.

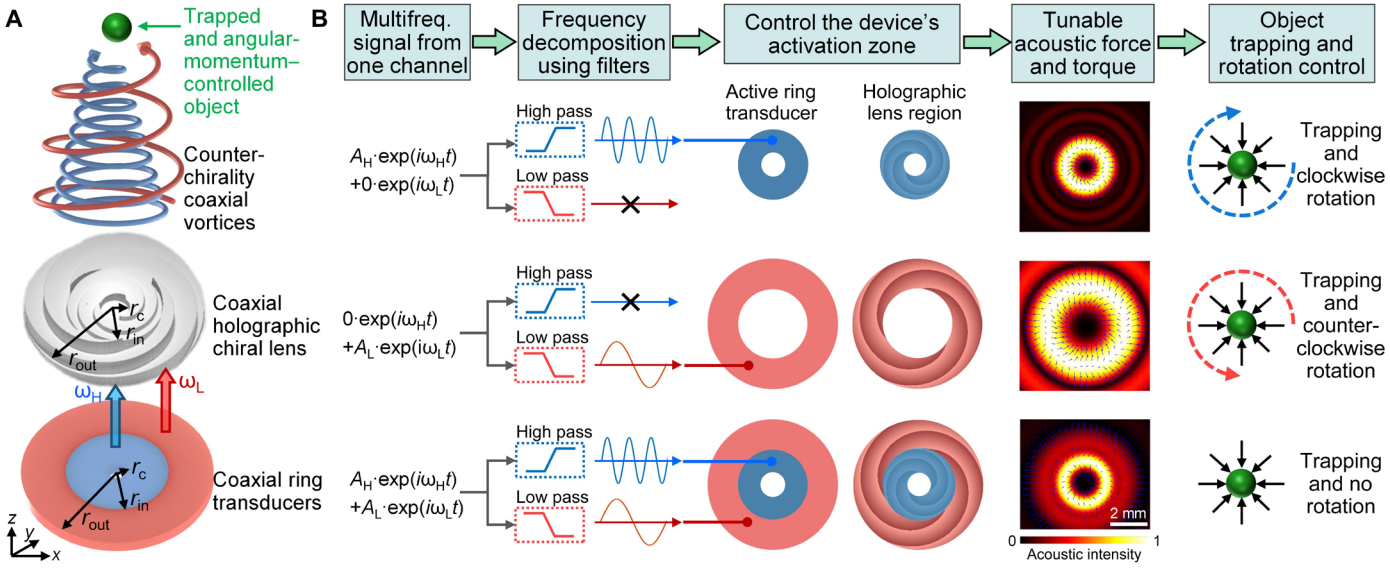

Fig. 2. Mechanism of chirality-tunable acoustic vortex tweezers. (**A**) Schematic of a chirality-tunable acoustic vortex tweezing device that is composed of coaxial ring transducers to generate incident acoustic waves with high and low frequencies ω_H and ω_L and a coaxial holographic chiral lens to transform incident waves to a chirality-tunable acoustic vortex beam. This beam has an acoustic potential well at the beam center to trap an object. By changing the excitation amplitudes A_H and A_L at frequencies ω_H and ω_L, the acoustic beam's angular momentum can be changed to control the trapped object's rotation. (**B**) Schematics showing three operation states for controlling the angular momentum of a trapped object. Top: When excitation amplitudes $A_H \neq 0$ and $A_L = 0$, the inner ring transducer is activated, and the waves at frequency ω_H transmit through the inner section of the lens to generate a vortex beam with a clockwise orbital angular momentum. This vortex beam can trap a particle at the vortex center and induce clockwise rotation. Middle: When excitation amplitudes $A_H = 0$ and $A_L \neq 0$, the outer ring transducer is activated to generate a vortex beam with a counterclockwise angular momentum, and this vortex beam can trap a particle and induce counterclockwise rotation. Bottom: When using optimized amplitudes $A_H \neq 0$ and $A_L \neq 0$, both the inner and outer ring transducers are activated, and the interaction of two acoustic vortices at different frequencies ω_H and ω_L leads to a potential well that enables stable object trapping. The torque applied to the particle can be minimized, so that the trapped particle has no rotation. Magnified views of acoustic fields are provided in fig. S2.

the thickness profile $h_{out}(\mathbf{x})$ of the lens outer section can transform an incident wave at ω_L to a confined vortex beam with a topological charge number of $-Q$. To facilitate the acoustic lens design, we established an analytical model of our chirality-tunable acoustic vortex device (see section S1) for quickly predicting the acoustic pressure and intensity fields that would be generated and the acoustic radiation forces that would be applied on small and large spheres. Details for determining the thickness profiles $h_{in}(\mathbf{x})$ and $h_{out}(\mathbf{x})$ of the coaxial holographic chiral lens are given in section S2.

Figure 2B shows the mechanism to tune the acoustic vortex tweezers' chirality for controlling the rotation of a trapped object. First, when a high-frequency signal $A_H e^{it\omega_H}$ is used to excite the inner ring transducer (see Fig. 2B, top row), waves at a frequency of ω_H are generated and then transmitted through the lens' inner section to form a focused vortex beam with a topological charge number of $+Q$ and a clockwise orbital angular momentum. Accordingly, acoustic tweezers are formed by the vortex center's potential well, which enables single-object trapping. The tweezers can also induce clockwise object rotation, as the clockwise acoustic angular momentum transfers to the object. Second, when a low-frequency signal $A_L e^{it\omega_L}$ is used to excite the outer ring transducer (see Fig. 2B, middle row), a focused vortex beam with a topological charge number of $-Q$ and a counterclockwise orbital angular momentum can be generated. Accordingly, the acoustic vortex–based tweezers can induce counterclockwise rotation of the trapped object. Third, when high- (ω_H) and low- (ω_L) frequency excitation signals are sent to the inner and outer ring transducers, respectively (see Fig. 2B, bottom row), two coaxial vortices with counter chiralities are generated at frequencies of ω_H and ω_L, respectively. The interaction of these counter-chirality acoustic vortices leads to a dual-frequency acoustic potential well to trap an object. Moreover, by adjusting the amplitude ratio A_H/A_L, the total angular momentum transferred to the trapped object can be minimized to achieve single-object trapping without rotation. To experimentally implement the aforementioned control method, a dual-frequency excitation signal generated from one set of wave signal generation equipment is decomposed to high- and low-frequency components using filters, and the decomposed high- and low-frequency components are then sent to the inner and outer ring transducers, respectively. The control method can also be implemented using two sets of signal generation equipment for exciting the inner and outer ring transducers, respectively.

Compared to previous acoustic vortex devices, our chirality-tunable acoustic vortex device offers the functions of changing the vortex chirality, switching the topological charge number, adjusting the acoustic wave's orbital angular momentum, and controlling the rotation (Ω_z) of a trapped object by simply adjusting the excitation amplitudes at frequencies of ω_H and ω_L, respectively. Moreover, compared to a mechanical robotic gripper, our acoustic vortex tweezers can be considered as a "contactless" gripper (or end effector) that can grab an object in a contact-free manner. By integrating our contactless acoustic end effector with a programmable robot, our system allows for 3D translation (u_x, u_y, and u_z) of an acoustically trapped object along complex 3D paths. Because the acoustic lenses used by our device are interchangeable, our acoustic vortex device

can generate various vortex beams to meet different requirements. For example, to manipulate an object with a specific size at a particular depth in a fluid, an acoustic lens can be readily designed using the approach detailed in section S2 and then fabricated through 3D printing in 0.5 hours. To demonstrate our technology, we designed and manufactured multiple lenses to successfully manipulate objects with sizes ranging from 75 μm to 5 mm, even in conditions with barriers between the acoustic devices and objects. Details of our experimental results are provided below.

4-DOF manipulation of single objects

Two fully functional, robot-assisted chirality-tunable acoustic vortex tweezing systems have been developed, by integrating acoustic vortex devices with a robotic arm and a high-resolution robotic linear motion stage (see fig. S1A and S1B for their photos). These two systems enable programmable, contactless, multifunctional, 4-DOF manipulation of single objects in liquids. Specifically, they can accomplish single-object trapping, controllable rotation of the trapped object, and programable translation of the trapped object along complex 3D paths. Moreover, our current systems offer features such as manipulation of different-sized (e.g., micro-to-millimeter) objects, high translation resolution (20 μm), and a large workspace (670 × 970 × 250 mm).

To demonstrate the versatile functions of the chirality-tunable acoustic vortex device, we performed a series of experiments. First, we demonstrated that our manufactured acoustic vortex device can change the generated vortex beam's chirality and control the trapped object's rotation by tuning the input amplitudes at low and high frequencies. As shown in the acquired acoustic fields (fig. S3) by a needle-type hydrophone on a 3D scanning stage, an acoustic vortex beam with a topological charge number of −3 and a counterclockwise orbital angular momentum is generated under a low-frequency (1.04 MHz) excitation. The acoustic field changes to a vortex beam with a topological charge number of +3 and a clockwise orbital angular momentum when changing the excitation to a high-frequency (3.35 MHz) signal. This ability to tune an acoustic wave's angular momentum ensures the control of a trapped object's rotation. To confirm this, we demonstrated that a 3-mm plastic sphere could be rotated in the clockwise direction, gradually stopped, and then rotated in the counterclockwise direction (see Fig. 3, A and B, and movie S1). We also found that the size of the acoustic vortex–based potential well can be gradually increased by increasing the topological charge number and/or reducing the wave frequency (see figs. S4 and S5). In addition, the acoustic radiation force applied on a sphere varies with the sphere's size, density, and sound speed (see fig. S6). By operating acoustic vortex devices with different frequencies and topological charge numbers, our robotic system can trap and manipulate different-sized objects. As validated by our experimental results (see Fig. 3C), plastic spheres with diameters of 3, 4, and 5 mm can be trapped in a 3D space by increasing the topological charge number from 3 to 4 and then to 5.

In addition to demonstrating the chirality-tunable acoustic vortex devices, a series of experiments were performed to validate some advanced functions enabled by the integrated robotic systems. First, we showed the ability to tilt the acoustic vortex beam direction using a robotic arm-assisted acoustic device. As shown in Fig. 3D, by gradually changing the tilt angle from 0° to 23.5° (i.e., the angle between the vortex beam axis and the z direction), a 3-mm plastic sphere can still be trapped by acoustic vortex tweezers. We also observed that the plastic sphere could not be trapped when the angle was larger than 23.5°. Above this angle, the vertical acoustic radiation force applied by a tilted vortex beam was not able to overcome the other forces such as buoyancy and gravity. Second, to demonstrate the capability of translating single objects along arbitrary-shaped paths in a 3D space in a contactless and programmable manner, our integrated system was used to successfully translate a 3-mm plastic sphere along a VT-shaped path in the x-y plane (movie S2), a VT-shaped path in the x-z plane (Fig. 3E and movie S3), and a 3D helical path (Fig. 3F and movie S4). Third, to demonstrate the high-resolution translation of single micro-objects, our integrated system was used to successfully translate a 75-μm polystyrene particle in the x-y plane to write the letters "VT" (see Fig. 3G and movie S5). According to our parametric study (see fig. S4), a higher frequency and a lower charge number result in a smaller potential well. Therefore, we used a vortex beam with a small charge number of 1 at a frequency of 3.35 MHz for the high-resolution writing of VT.

Through-biological-barrier acoustic tweezers

Although optical tweezers can achieve high-precision manipulation of small objects, they have difficulty penetrating thick tissues and bones (*6*). Magnetic tweezers have been used for manipulating objects in regions with biological barriers such as transporting objects along blood vessels to target locations (*64*–*67*); however, magnetic tweezing methods are most effective when manipulating objects with high relative permeabilities (e.g., objects containing iron), which excludes many biological objects of interest. Because acoustic waves can efficiently apply forces on various objects with a wide range of material properties (such as cells, bubbles, polymer particles, metal particles, etc.) and penetrate thick tissues and rigid bones, we believe that acoustic tweezers have great potential for manipulating diverse types of objects even in spaces shielded with tissue and bone barriers.

Using our acoustic vortex tweezing device, we confirmed that the generated acoustic vortex beam could successfully transmit through a sample of pork belly (~6 mm thick) to trap a 3-mm plastic sphere (see Fig. 4A and movie S6). Second, we validated that the acoustic vortex beam generated by our device can transmit through a heterogeneous material barrier for single object manipulation. The pressure acoustic field scanning results indicate that an acoustic vortex beam (Fig. 4D) can transmit through a real monkey skull (~1.6 mm thick) and generate an acoustic vortex–based potential well (Fig. 4, E and F) to create acoustic tweezers. The acquired photo (Fig. 4B) and movie S7 show that acoustic vortex tweezers can be formed in a 3D space shielded by a skull barrier to trap and suspend a 1-mm plastic cube. Third, using the integrated robot-assisted acoustic vortex tweezing system, we demonstrated the translation of a 3-mm plastic sphere inside a Y-shaped channel in a 36-mm-thick synthetic gelatin phantom (fig. S7D) that was fabricated for mimicking a branched blood vessel within soft tissue. As shown in Fig. 4G and movie S8, the 3-mm plastic sphere can be successfully translated from the main branch into the lower branch and then into the upper branch by using the contactless acoustic vortex tweezers integrated with a high-precision robotic motion platform. To achieve the aforementioned object manipulation abilities, e.g., penetrating tissue and skulls to manipulate objects far from the acoustic vortex device, multiple factors should be considered when designing the device. (i) It is preferential that the operational frequency is in a low-frequency range (e.g., 500 kHz to 1 MHz), as low-frequency acoustic waves have lower energy loss in biological materials compared to high-frequency waves. (ii) The transducer's diameter should be large

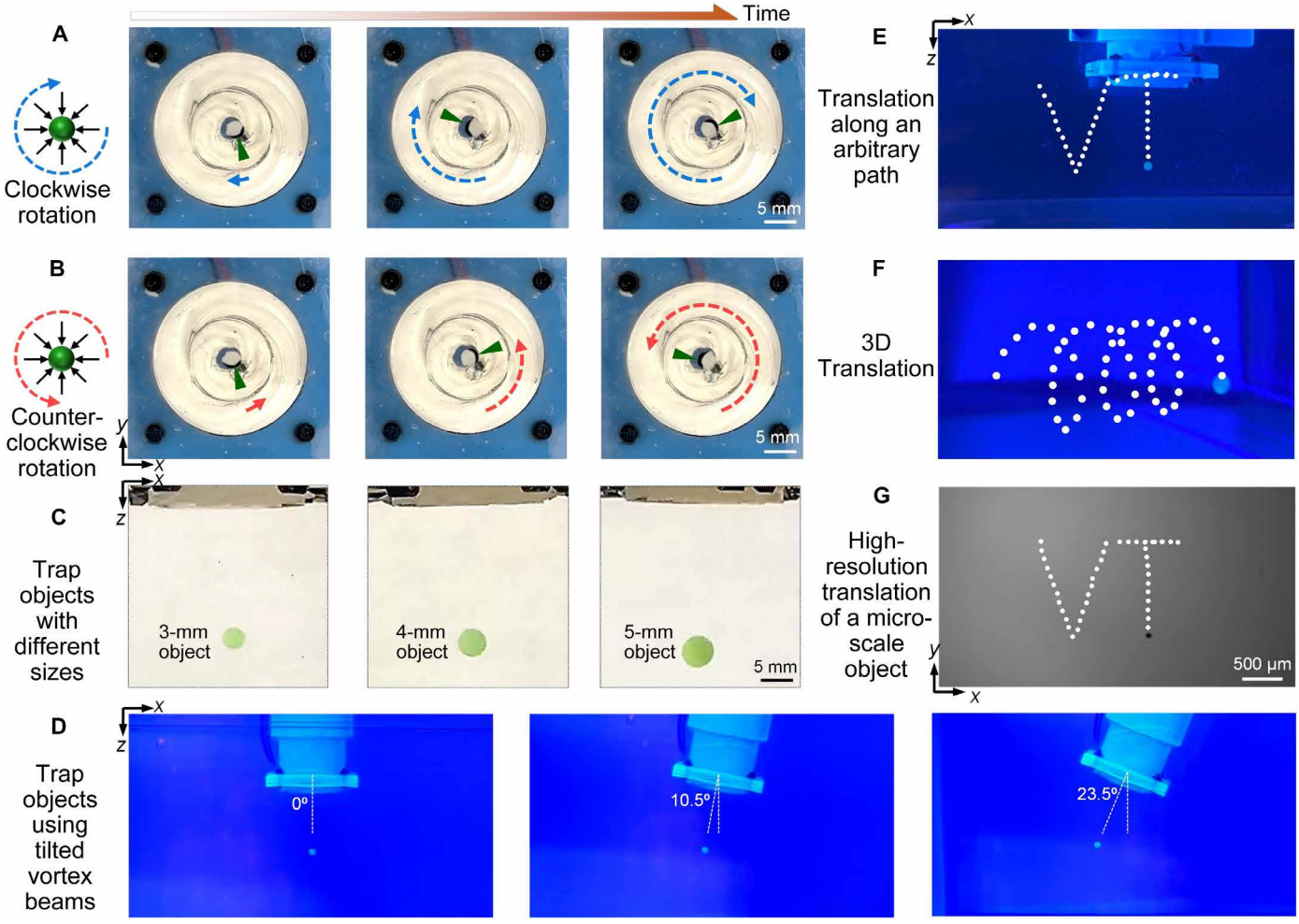

Fig. 3. Contactless, multifunctional, 4-DOF manipulation of single objects. (**A** and **B**) Time-sequential photos showing that a 3-mm plastic sphere was trapped at the vortex center and rotated in the clockwise and counterclockwise directions at the excitation frequencies of 3.35 and 1.04 MHz, respectively. (**C**) Photos showing plastic spheres with different diameters of 3, 4, and 5 mm can be trapped by 1.04-MHz acoustic vortex beams with different topological charge numbers of 3, 4, and 5. (**D**) Photos showing a 3-mm plastic sphere can be trapped using tilted acoustic vortex beams. For this experiment, the acoustic device is attached to the end of a robotic arm. (**E**) Translation of a 3-mm plastic particle in the *x*-*z* plane to write the letters VT. (**F**) Translation of a 3-mm plastic particle along a 3D helical path. (**G**) High-resolution translation of a 75-μm polystyrene particle in the *x*-*y* plane to write the letters VT. The white dots indicate the actual positions of the sphere during the translation process.

enough, so that the generated focused vortex beam can reach the target object even when it is far away (e.g., several centimeters). (iii) A high-efficiency acoustic transducer is preferred, as the acoustic device needs to deliver sufficient energy through the barrier to the particle trapping position. The in vitro experimental results in this study prove the feasibility of using our acoustic system to achieve contactless, programmable translation of small objects in 3D spaces with real tissue and skull barriers. This work lays the foundation for developing advanced acoustic-based technologies for achieving in vitro and even in vivo, programmable, 3D acoustic object manipulation.

Live ultrasound imaging–assisted acoustic tweezers

Although acoustic tweezers can perform certain contactless object manipulation, most acoustic tweezing systems, which typically use live optical cameras for monitoring the object's movements, are limited to manipulating objects in transparent media (*10*–*21*, *53*, *57*). The reliance on optical cameras makes it difficult to realize controllable manipulation of objects in nontransparent environments, such as objects suspended in opaque media or objects in spaces with nontransparent barriers (such as those in regions shielded by the skull or thick tissue). Inspired by ultrasound imaging–guided intervention technologies, which use ultrasound imaging to provide images that help physicians visualize and target surgical sites, this study presents live ultrasound imaging–assisted acoustic vortex tweezers. Our approach addresses the limitations of traditional acoustic tweezers guided by optical camera images and opens the opportunity for precise manipulation of objects in nontransparent environments.

Our ultrasound imaging–assisted acoustic vortex tweezing approach integrates an ultrasound phased array imaging technique with our developed robot-assisted vortex acoustic tweezers (see Fig. 5A for a schematic and fig. S8 for a test photo). An ultrasound phased array system, which is synchronized with the acoustic tweezing device, uses a 128-element phased-array probe and a customized fast imaging algorithm (section S3) to generate live ultrasound

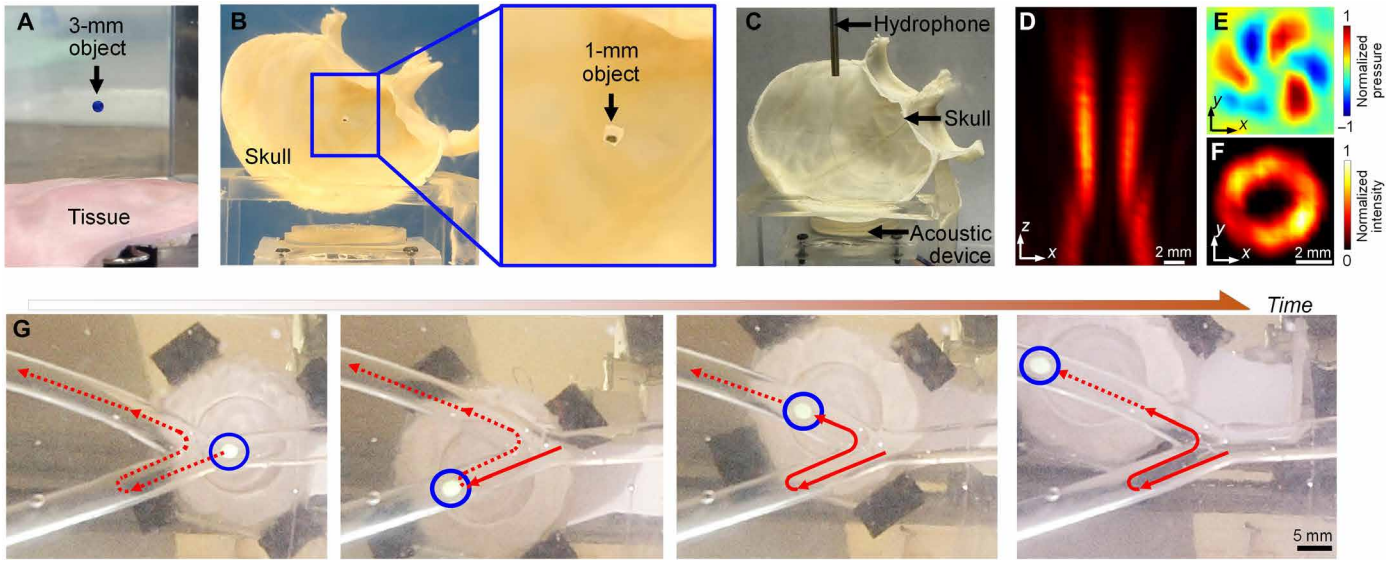

Fig. 4. Manipulation of single objects shielded by biological barriers. (**A**) Photo showing a 3-mm plastic sphere trapped by an acoustic vortex beam transmitted through a pork belly (~6 mm thick). (**B**) Photo showing a 1-mm plastic cube trapped by an acoustic vortex beam transmitted through a monkey skull (~1.6 mm thick). (**C**) Experimental setup for characterizing the acoustic vortex beam transmitted through a monkey skull. (**D**) Acquired acoustic intensity field in the *x*-*z* plane. (**E** and **F**) Acquired acoustic pressure and intensity fields in a horizontal plane 30 mm away from the holographic lens. These characterization results prove that the generated acoustic vortex beam can transmit through a monkey skull and generate an acoustic potential well to trap a particle. (**G**) Time-sequential photos showing a 3-mm plastic sphere trapped by an acoustic vortex beam and translated inside a branched channel of a 36-mm-thick biomimetic synthetic gelatin phantom that mimics the tissue with a branched blood vessel. The sphere was translated from the main branch into the lower branch and then into the upper branch.

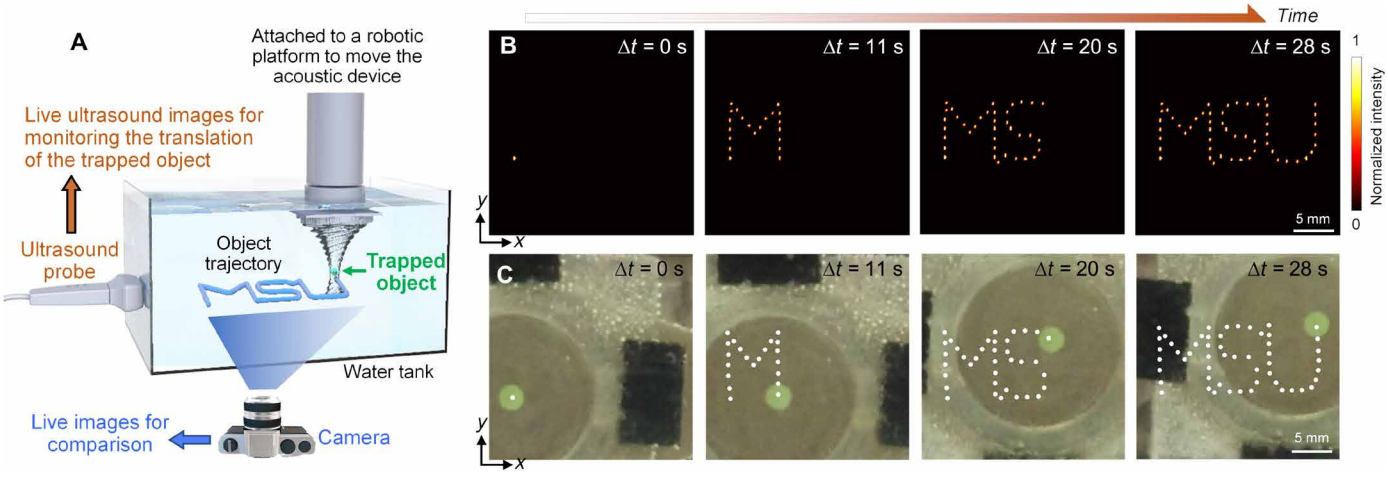

Fig. 5. Ultrasound imaging–assisted acoustic vortex tweezers. (**A**) Schematic of a test setup that has robot-assisted acoustic vortex tweezers for contactless object manipulation, a linear phased array probe outside a water tank for monitoring the object motion using live ultrasound images, and a camera under the water tank to acquire live images for comparison. (**B**) Stacked ultrasound images showing the positions and moving trajectory of a 3-mm plastic sphere that was trapped by acoustic waves and translated to write three letters MSU. (**C**) Time-sequential photos showing a 3-mm plastic sphere translated to write three letters MSU. The white dots indicate the sphere's actual positions during the translation process.

images for monitoring the acoustic vortex tweezer-based object manipulation process. In particular, our imaging algorithm minimizes the required pulse-echo cycles for collecting ultrasound signals and implements a frequency-domain filtering step to remove acoustic tweezer–induced signal noise. To demonstrate the effectiveness of the ultrasound imaging–assisted acoustic vortex tweezers, we used our integrated system to translate a 3-mm plastic sphere, which was suspended in a water tank, along a complex path to write the letters "MSU." During the acoustic manipulation experiment, the ultrasound phased array system generated live ultrasound images to monitor the object's movement, and an optical camera was used to record its trace for comparison. The acquired ultrasound image (Fig. 5B, left) shows a high-intensity spot that indicates the initial position of the acoustically trapped particle. The stacked ultrasound images (Fig. 5B, middle and right) show particle positions at different moments and the particle moving trajectory that depicts three

letters MSU. The dynamic manipulation process can be seen in movie S9, generated by combining ultrasonic images acquired at different moments of the object manipulation process. Figure 5C shows time-sequential photos selected from a video (movie S9) recorded by an optical camera during the acoustic tweezer–based object manipulation process. By comparing Fig. 5B and Fig. 5C, it can be seen that the particle trajectory recorded by ultrasound imaging agrees with the particle path recorded by the optical camera. Our experiment verifies that the ultrasound imaging–assisted acoustic vortex tweezers are able to generate live ultrasound images for monitoring the invisible acoustic tweezer–controlled contactless particle manipulation process. We believe that this capability will greatly benefit the contactless, precision manipulation of objects in nontransparent environments, improving the in vivo application potential of this technology.

DISCUSSION

In this study, we developed robot-assisted, chirality-tunable acoustic vortex tweezing systems that enable contactless, multifunctional, high-resolution, 4-DOF manipulation of micro to millimeter-sized single objects in large 3D spaces. Particularly, our technique leverages a unique chirality-tunable acoustic vortex tweezing device, which uses a coaxial holographic chiral lens to transform incident waves at frequencies of ω_H and ω_L to coaxial focused acoustic vortex beams with counter topological charge numbers $+Q$ and $-Q$. At a fundamental level, this acoustic device opens up opportunities for producing next-generation designs that have a higher degree of control over acoustic vortex beams. By adjusting the excitation amplitudes at frequencies of ω_H and ω_L, our acoustic device is able to change the vortex chirality, switch the topological charge number, and adjust the acoustic wave's orbital angular momentum. We expect our device design to inspire researchers to develop coaxial acoustic vortex devices for studying coaxial vortex-vortex interaction. Moreover, our acoustic device enables the functionality of controlling the rotation (Ω_z) of acoustically trapped single objects in liquids. The validation experiment shows that a plastic sphere can be rotated in the clockwise direction, stopped, and then rotated in the counterclockwise direction. This functionality could prove useful in acoustic tweezer–assisted imaging of objects from different angles by rotating the objects and bottom-up fabrication of microscale assemblies with the orientation of each element being well controlled. Furthermore, we developed fully functional, robot-assisted, acoustic tweezing systems by integrating acoustic tweezing devices, which could be considered as contactless grippers (or robotic end effectors) to grab single objects in a contact-free manner, with programmable robots to translate and tilt the acoustic tweezering devices. Our developed fully functional systems enable 3D translation (u_x, u_y, and u_z) of acoustically trapped micro- to millimeter-sized single objects along complex 3D paths. The validation experiments show successful translations of a 3-mm plastic sphere along a 3D helical path and the translations of a 75-μm polystyrene particle to write the high-resolution letters VT. Even with these successes, our acoustic device has not been integrated with high-resolution fluorescence microscopy systems, limiting the ability to manipulate and observe smaller objects as well as perform fluorescent imaging of objects during manipulation. In addition, to manipulate smaller micro-objects, acoustic vortex beams at high frequencies (e.g., >10 MHz) with smaller potential wells are preferred. To push the frequency limit of our acoustic tweezers, high-resolution 3D printing (e.g., two-photon polymerization) is critical for fabricating holographic acoustic lenses with precise architectures encoded with the desired spatial phase profiles.

Our device is able to trap and manipulate single objects in 3D spaces shielded by biological barriers (such as tissue or skull) by sending acoustic vortex beams through the biological materials. This ability was demonstrated through a series of in vitro experiments that used acoustic tweezers to manipulate single objects in regions with three different barriers. First, we confirmed the generation of through-skull acoustic vortex tweezers that could trap a 1-mm plastic cube in a 3D space with a ~1.6-mm-thick skull barrier. The acoustic field scanning results prove the successful generation of a focused acoustic vortex beam with the desired topological charge number and potential well shape after the acoustic waves transmitting through the real skull. Second, we showed that acoustic vortex tweezers could be generated to trap and suspend a 3-mm plastic sphere after the acoustic waves transmitting through a ~6-mm-thick pork belly. Third, we demonstrated that acoustic vortex tweezers could be generated to trap and translate a 3-mm plastic sphere along a complex path inside a Y-shaped channel within a 36-mm-thick synthetic gelatin phantom, which mimics soft tissue with a branched blood vessel. The aforementioned tests are limited to scenarios, where the vortex beams are normal to the barriers. When the vortex beams are not incident normally, it becomes more challenging to manipulate objects shielded by barriers. Multiple factors affect acoustic object manipulation, such as wave refraction because of the sound speed change at the barrier, wave energy reflection depending on the impedance change and the incident angle, acoustic energy loss in the barrier, and nonuniform transmission phase changes related to the barrier's spatially varying thickness profile and material properties. To compensate for the nonuniform phase changes, a potential solution is introducing additional phase shifts to the acoustic lens. Through future experiments and simulations, we will investigate cases where the biological barriers are not perpendicular to the acoustic beams to better understand the limitations of acoustic vortex–based manipulation of objects shielded by biological barriers.

As a final demonstration of our technology, ultrasound imaging–assisted acoustic vortex tweezers were achieved by integrating an ultrasonic phased array, robot-assisted acoustic vortex tweezers, and a customized imaging approach that minimizes the required pulse-echo cycles for sensing and removes acoustic tweezer–induced noises. Through proof-of-concept experiments, we showed that the acoustic vortex tweezer–based contactless object manipulation process could be monitored by using live ultrasound phased array imaging. During experimentation, the live phased array images showed the step-by-step translation process of a 3-mm plastic sphere along a complex MSU-shaped trajectory.

With the aforementioned object manipulation capabilities, this work on acoustic vortex tweezers moves a step forward toward the development of next-generation robotic systems that can achieve multifunctional, high-DOF, high-resolution, contactless manipulation of micro- to millimeter-sized objects made of different materials. We believe that the successful development of this type of robotic platform will advance a wide range of applications, such as contactless handling of delicate biological samples (e.g., embryos, worms, zebrafishes, etc.) for separation and sorting, translation of objects in regions with biological barriers (e.g., tissue and skull), arranging of micro-objects for controlling self-assembly, and arranging cell distributions for biomanufacturing. To further push the boundary of this work,

our future research will investigate the manipulation of more biological samples such as cells, embryos, worms, and zebrafish; we will test our approach for manipulating objects in flowing media; and we will explore applications in biomedical engineering and advanced manufacturing.

MATERIALS AND METHODS

Analytical simulations

To predict the acoustic pressure, energy, and radiation force fields generated by a chirality-tunable acoustic vortex device, an analytical model of the device was established. The details of the analytical model are given in section S1 and fig. S9. Based on the analytical model, we developed Matlab codes to quickly simulate the acoustic pressure, energy, and radiation force fields for chirality-tunable acoustic vortex devices working at different conditions such as different input amplitudes and frequencies.

Design, fabrication, and operation of acoustic vortex devices

Each acoustic vortex tweezing device is composed of a holographic chiral lens (see fig. S1C) and piezoelectric ring transducers (Steiner & Martins Inc.). The acoustic lens' thickness profile (see fig. S10) is obtained by using the desired position-dependent phase shifts that can be calculated using the method presented in section S2. The lens was fabricated using a high-resolution stereolithography 3D printer (Form 3, Formlabs) with a photocurable resin (RS-F2-GPCL-04, Formlabs). The first- and second-order thickness-mode resonant frequencies of the used piezoelectric transducers are 1.04 and 3.35 MHz, respectively. For each acoustic vortex device, the holographic chiral lens and the piezoelectric transducers are coupled through a thin (~0.2-mm-thick) ultrasound couplant layer. To drive the acoustic vortex device, an input signal with two frequency components (1.04 and 3.35 MHz) is generated by a function generator (AFG3102C, Tektronix Inc.) and then amplified by a power amplifier (A075, Electronics & Innovation Ltd.). The amplified dual-frequency voltage signal is decomposed into low- (1.04 MHz) and high- (3.35 MHz) frequency components using a customized circuit (see fig. S11), and the low- and high-frequency components are sent to the outer and inner ring transducers to generate acoustic vortices with different angular momenta. By changing the amplitudes A_L and A_H for the low- and high-frequency components, the total acoustic field's angular momentum can be tuned, and the trapped object's rotational motion can be controlled to achieve three states: clockwise rotation, counterclockwise rotation, and trapping with no rotation. In our experiments, to manipulate 3-, 4-, and 5-mm plastic spheres without biological barriers between acoustic devices and spheres, the voltages applied to the transducers are ($A_L = 25.2$ V, $A_H = 0$), ($A_L = 29.0$ V, $A_H = 0$), and ($A_L = 33.4$ V, $A_H = 0$), respectively. To trap a 3-mm plastic sphere without inducing rotation, the voltages applied to the transducers are ($A_L = 23.4$ V, $A_H = 32.5$ V). To manipulate a 75-μm polystyrene particle, the voltages applied to the transducers are ($A_L = 0$, $A_H = 35.6$ V). To manipulate a 3-mm sphere with a pork belly barrier, a 1-mm plastic cube with a monkey skull barrier, and a 3-mm sphere in a phantom, the voltages applied to the transducers are ($A_L = 34.4$ V, $A_H = 0$), ($A_L = 35.6$ V, $A_H = 0$), and ($A_L = 32.9$ V, $A_H = 0$), respectively.

Integration with robotic systems

The fabricated acoustic vortex devices are integrated with two different robotic platforms including a robotic arm (Elephant Robotics) shown in fig. S1A and a customized 3D linear motion stage shown in fig. S1B. The linear motion stage is controlled by a motion controller (OpenBuilds) with a microstepping function for high-resolution object manipulation. For example, this design allows for translating a 75-μm polystyrene sphere along a microscale path to write the letters VT. To mount acoustic vortex devices on these robotic systems, we used customized fixtures manufactured through 3D printing. To automatically move the acoustically trapped particle along desired paths, Python codes were developed to control the robotic arm, and MATLAB codes were developed to control the 3D linear motion stage through serial communication.

Preparation of samples for manipulating objects shielded by biological barriers

Multiple samples were prepared to demonstrate acoustic manipulation of objects shielded by biological barriers. The pork belly (~6 mm thick) was purchased from a local grocery store. The monkey skull (~1.6 mm thick; provided by Atlantic Coral Enterprise Inc.) was characterized by x-ray computed tomography (XT H 225 ST, Nikon, Japan). The 3D and cross-sectional views of the skull are given in fig. S7 (A to C). To manufacture a sample that can mimic a tissue with branched blood vessels, a biomimetic phantom (155 mm by 140 mm by 36 mm; see fig. S7D) was fabricated through a molding process using synthetic gelatin. This phantom has a Y-shaped channel at a depth of 18 mm. A 3-mm plastic sphere was loaded into the channel with water for contactless acoustic manipulation experiments.

Acoustic field characterization

The acoustic field characterization experiments were performed using a hydrophone (HNR-0500, ONDA Co.) mounted on a customized 3D linear motion stage, as illustrated in fig. S12. The hydrophone was connected to an oscilloscope (SDS 1202X-E, SIGLENT Technologies) to acquire time-domain waveforms. A function generator (AFG3102C, Tektronix Inc.) was used to send excitation signals to acoustic devices to be characterized. The linear motion stage, function generator, and oscilloscope were all synchronized and controlled by a customized MATLAB program through serial communication. To acquire an acoustic field, point-by-point scanning was performed, by gradually changing the hydrophone position and acquiring acoustic pressure waveforms. At each measurement position, 16 waveforms were acquired and then averaged to obtain a denoised waveform $s(t)$. By combining averaged waveforms acquired at all the positions in the desired characterization region, we obtained a time-space wave field $S_{ts}(t, x, y, z)$ representing the propagation of acoustic waves. By further applying the Fourier transform to the acquired data, we obtained a frequency-space wave field $S_{fs}(f, x, y, z)$, which is a complex number field function. The acoustic wave intensity field at a selected frequency of f_i can be evaluated by $|S_{fs}(f_i, x, y, z)|^2$.

Image and video acquisition

To acquire bright-field images and videos during acoustic particle manipulation experiments, we used a waterproof camera (Osmo Action 3, DJI Technology Co., China). To acquire microscopic images and videos for monitoring the manipulation of a 75-μm polystyrene particle, we used a camera (MTR3CMOS07100KMA, ToupCam) attached to a 4× objective lens. To acquire ultrasound images, a linear phased array probe with 128 elements (L7-4, Philips) was connected to an ultrasound data acquisition system (Vantage 64, Verasonics) with 64 independent receiver channels. Using this system, we could

send excitation signals to the phased array probe and record ultrasonic signals from individual elements of the probe. With all the acquired signals, ultrasonic images were constructed by using our customized imaging algorithms (see section S3). In particular, to maximize the imaging speed for live ultrasound imaging, our array imaging scheme (fig. S13) only needs two pulse-echo cycles to create an ultrasound image (i.e., one imaging frame). In the first cycle, all the 128 elements are simultaneously excited to generate a plane incident wave pulse, and elements 1 to 64 are used to acquire signals of backscattering waves from an object (e.g., acoustically trapped 3-mm plastic sphere). In the second cycle, the same pulse-echo process is repeated with the elements 65 to 128 for acquiring signals of backscattering waves. Using our customized imaging algorithms (section S3) to process all the acquired waveforms, an ultrasound image can be quickly constructed. By repeating the aforementioned imaging process, we can acquire a series of ultrasound images at different times for monitoring the acoustic-based object manipulation process. These time-sequential images can also be combined to output a video showing the dynamic particle manipulation process.

Supplementary Materials

This PDF file includes:

Sections S1 to S3
Figs. S1 to S13
Table S1
Legends for movies S1 to S9
References

Other Supplementary Material for this manuscript includes the following:

Movies S1 to S9

REFERENCES AND NOTES

1. G. Bao, S. Suresh, Cell and molecular mechanics of biological materials. *Nat. Mater.* **2**, 715–725 (2003).
2. D. G. Grier, A revolution in optical manipulation. *Nature* **424**, 810–816 (2003).
3. J. Voldman, Electrical forces for microscale cell manipulation. *Annu. Rev. Biomed. Eng.* **8**, 425–454 (2006).
4. I. De Vlaminck, C. Dekker, Recent advances in magnetic tweezers. *Annu. Rev. Biophys.* **41**, 453–472 (2012).
5. A. Ozcelik, J. Rufo, F. Guo, Y. Gu, P. Li, J. Lata, T. J. Huang, Acoustic tweezers for the life sciences. *Nat. Methods* **15**, 1021–1028 (2018).
6. K. Dholakia, B. W. Drinkwater, M. Ritsch-Marte, Comparing acoustic and optical forces for biomedical research. *Nat. Rev. Phys.* **2**, 480–491 (2020).
7. A. Ashkin, J. M. Dziedzic, T. Yamane, Optical trapping and manipulation of single cells using infrared-laser beams. *Nature* **330**, 769–771 (1987).
8. M. Krishnan, N. Mojarad, P. Kukura, V. Sandoghdar, Geometry-induced electrostatic trapping of nanometric objects in a fluid. *Nature* **467**, 692–695 (2010).
9. S. H. Leuba, M. A. Karymov, M. Tomschik, R. Ramjit, P. Smith, J. Zlatanova, Assembly of single chromatin fibers depends on the tension in the DNA molecule: Magnetic tweezers study. *Proc. Natl. Acad. Sci. U.S.A.* **100**, 495–500 (2003).
10. J. R. Wu, Acoustical tweezers. *J. Acoust. Soc. Am.* **89**, 2140–2143 (1991).
11. D. Foresti, M. Nabavi, M. Klingauf, A. Ferrari, D. Poulikakos, Acoustophoretic contactless transport and handling of matter in air. *Proc. Natl. Acad. Sci. U.S.A.* **110**, 12549–12554 (2013).
12. A. Marzo, S. A. Seah, B. W. Drinkwater, D. R. Sahoo, B. Long, S. Subramanian, Holographic acoustic elements for manipulation of levitated objects. *Nat. Commun.* **6**, 8661 (2015).
13. K. Melde, A. G. Mark, T. Qiu, P. Fischer, Holograms for acoustics. *Nature* **537**, 518–522 (2016).
14. K. Melde, E. Choi, Z. G. Wu, S. Palagi, T. Qiu, P. Fischer, Acoustic fabrication via the assembly and fusion of particles. *Adv. Mater.* **30**, 201704507 (2018).
15. H. G. Lim, K. K. Shung, Quantification of inter-erythrocyte forces with ultra-high frequency (410 MHz) single beam acoustic tweezer. *Ann. Biomed. Eng.* **45**, 2174–2183 (2017).
16. K. H. Lam, Y. Li, Y. Li, H. G. Lim, Q. F. Zhou, K. K. Shung, Multifunctional single beam acoustic tweezer for non-invasive cell/organism manipulation and tissue imaging. *Sci. Rep.* **6**, 37554 (2016).
17. J. Dual, T. Schwarz, Acoustofluidics 3: Continuum mechanics for ultrasonic particle manipulation. *Lab Chip* **12**, 244–252 (2012).
18. D. Carugo, T. Octon, W. Messaoudi, A. L. Fisher, M. Carboni, N. R. Harris, M. Hill, P. Glynne-Jones, A thin-reflector microfluidic resonator for continuous-flow concentration of microorganisms: a new approach to water quality analysis using acoustofluidics. *Lab Chip* **14**, 3830–3842 (2014).
19. A. Marzo, M. Caleap, B. W. Drinkwater, Acoustic virtual vortices with tunable orbital angular momentum for trapping of mie particles. *Phys. Rev. Lett.* **120**, 044301 (2018).
20. M. A. Ghanem, A. D. Maxwell, Y.-N. Wang, B. W. Cunitz, V. A. Khokhlova, O. A. Sapozhnikov, M. R. Bailey, Noninvasive acoustic manipulation of objects in a living body. *Proc. Natl. Acad. Sci. U.S.A.* **117**, 16848–16855 (2020).
21. Y. Yang, Y. Yang, D. Liu, Y. Wang, M. Lu, Q. Zhang, J. Huang, Y. Li, T. Ma, F. Yan, H. Zheng, In-vivo programmable acoustic manipulation of genetically engineered bacteria. *Nat. Commun.* **14**, 3297 (2023).
22. J. Friend, L. Y. Yeo, Microscale acoustofluidics: Microfluidics driven via acoustics and ultrasonics. *Rev. Mod. Phys.* **83**, 647–704 (2011).
23. Y. Q. Fu, J. K. Luo, N. T. Nguyen, A. J. Walton, A. J. Flewitt, X. T. Zu, Y. Li, G. McHale, A. Matthews, E. Iborra, H. Du, W. I. Milne, Advances in piezoelectric thin films for acoustic biosensors, acoustofluidics and lab-on-chip applications. *Prog. Mater. Sci.* **89**, 31–91 (2017).
24. B. W. Drinkwater, Dynamic-field devices for the ultrasonic manipulation of microparticles. *Lab Chip* **16**, 2360–2375 (2016).
25. J. Rufo, P. Zhang, R. Zhong, L. P. Lee, T. J. Huang, A sound approach to advancing healthcare systems: The future of biomedical acoustics. *Nat. Commun.* **13**, 3459 (2022).
26. M. Wu, Y. Ouyang, Z. Wang, R. Zhang, P. H. Huang, C. Chen, H. Li, P. Li, D. Quinn, M. Dao, S. Suresh, Y. Sadovsky, T. J. Huang, Isolation of exosomes from whole blood by integrating acoustics and microfluidics. *Proc. Natl. Acad. Sci. U.S.A.* **114**, 10584–10589 (2017).
27. M. Rezeli, O. Gidlof, M. Evander, P. Bryl-Gorecka, R. Sathanoori, P. Gilje, K. Pawlowski, P. Horvatovich, D. Erlinge, G. Marko-Varga, T. Laurell, Comparative proteomic analysis of extracellular vesicles isolated by acoustic trapping or differential centrifugation. *Anal. Chem.* **88**, 8577–8586 (2016).
28. F. Guo, P. Li, J. B. French, Z. M. Mao, H. Zhao, S. X. Li, N. Nama, J. R. Fick, S. J. Benkovic, T. J. Huang, Controlling cell-cell interactions using surface acoustic waves. *Proc. Natl. Acad. Sci. U.S.A.* **112**, 43–48 (2015).
29. J. P. Lata, F. Guo, J. S. Guo, P. H. Huang, J. Yang, T. J. Huang, Surface acoustic waves grant superior spatial control of cells embedded in hydrogel fibers. *Adv. Mater.* **28**, 8632–8638 (2016).
30. S. M. Naseer, A. Manbachi, M. Samandari, P. Walch, Y. Gao, Y. S. Zhang, F. Davoudi, W. Wang, K. Abrinia, J. M. Cooper, A. Khademhosseini, S. R. Shin, Surface acoustic waves induced micropatterning of cells in gelatin methacryloyl (GelMA) hydrogels. *Biofabrication* **9**, 015020 (2017).
31. B. Kang, J. Shin, H. J. Park, C. Rhyou, D. Kang, S. J. Lee, Y. S. Yoon, S. W. Cho, H. Lee, High-resolution acoustophoretic 3D cell patterning to construct functional collateral cylindroids for ischemia therapy. *Nat. Commun.* **9**, 5402 (2018).
32. C. Bouyer, P. Chen, S. Guven, T. T. Demirtas, T. J. F. Nieland, F. Padilla, U. Demirci, A bio-acoustic levitational (BAL) assembly method for engineering of multilayered, 3D brain-like constructs, using human embryonic stem cell derived neuro-progenitors. *Adv. Mater.* **28**, 161–167 (2016).
33. J. P. K. Armstrong, J. L. Puetzer, A. Serio, A. G. Guex, M. Kapnisi, A. Breant, Y. Zong, V. Assal, S. C. Skaalure, O. King, T. Murty, C. Meinert, A. C. Franklin, P. G. Bassindale, M. K. Nichols, C. M. Terracciano, D. W. Hutmacher, B. W. Drinkwater, T. J. Klein, A. W. Perriman, M. M. Stevens, Engineering anisotropic muscle tissue using acoustic cell patterning. *Adv. Mater.* **30**, e1802649 (2018).
34. D. Ahmed, A. Ozcelik, N. Bojanala, N. Nama, A. Upadhyay, Y. C. Chen, W. Hanna-Rose, T. J. Huang, Rotational manipulation of single cells and organisms using acoustic waves. *Nat. Commun.* **7**, 11085 (2016).
35. C. Chen, Y. Gu, J. Philippe, P. Zhang, H. Bachman, J. Zhang, J. Mai, J. Rufo, J. F. Rawls, E. E. Davis, N. Katsanis, T. J. Huang, Acoustofluidic rotational tweezing enables high-speed contactless morphological phenotyping of zebrafish larvae. *Nat. Commun.* **12**, 1118 (2021).
36. V. M. Jooss, J. S. Bolten, J. Huwyler, D. Ahmed, In vivo acoustic manipulation of microparticles in zebrafish embryos. *Sci. Adv.* **8**, eabm2785 (2022).
37. M. Antfolk, C. Magnusson, P. Augustsson, H. Lilja, T. Laurell, Acoustofluidic, label-free separation and simultaneous concentration of rare tumor cells from white blood cells. *Anal. Chem.* **87**, 9322–9328 (2015).
38. P. Li, Z. M. Mao, Z. L. Peng, L. L. Zhou, Y. C. Chen, P. H. Huang, C. I. Truica, J. J. Drabick, W. S. El-Deiry, M. Dao, S. Suresh, T. J. Huang, Acoustic separation of circulating tumor cells. *Proc. Natl. Acad. Sci. U.S.A.* **112**, 4970–4975 (2015).
39. M. A. Burguillos, C. Magnusson, M. Nordin, A. Lenshof, P. Augustsson, M. J. Hansson, E. Elmer, H. Lilja, P. Brundin, T. Laurell, T. Deierborg, Microchannel acoustophoresis does not impact survival or function of microglia, leukocytes or tumor cells. *PLOS ONE* **8**, e64233 (2013).
40. S. X. Li, F. Guo, Y. C. Chen, X. Y. Ding, P. Li, L. Wang, C. E. Cameron, T. J. Huang, Standing surface acoustic wave based cell coculture. *Anal. Chem.* **86**, 9853–9859 (2014).

41. Y. Kurashina, K. Takemura, J. Friend, Cell agglomeration in the wells of a 24-well plate using acoustic streaming. *Lab Chip* **17**, 876–886 (2017).
42. P. Liu, Z. Tian, K. Yang, D. Naquin Ty, N. Hao, H. Huang, J. Chen, Q. Ma, H. Bachman, P. Zhang, X. Xu, J. Hu, J. Huang Tony, Acoustofluidic black holes for multifunctional in-droplet particle manipulation. *Sci. Adv.* **8**, eabm2592 (2022).
43. P. Liu, Z. Tian, N. Hao, H. Bachman, P. Zhang, J. Hu, T. J. Huang, Acoustofluidic multi-well plates for enrichment of micro/nano particles and cells. *Lab Chip* **20**, 3399–3409 (2020).
44. A. Del Campo Fonseca, C. Glück, J. Droux, Y. Ferry, C. Frei, S. Wegener, B. Weber, M. El Amki, D. Ahmed, Ultrasound trapping and navigation of microrobots in the mouse brain vasculature. *Nat. Commun.* **14**, 5889 (2023).
45. Y. Deng, A. Paskert, Z. Zhang, R. Wittkowski, D. Ahmed, An acoustically controlled helical microrobot. *Sci. Adv.* **9**, eadh5260 (2023).
46. D. Ahmed, M. Lu, A. Nourhani, P. E. Lammert, Z. Stratton, H. S. Muddana, V. H. Crespi, T. J. Huang, Selectively manipulable acoustic-powered microswimmers. *Sci. Rep.* **5**, 9744 (2015).
47. S. Sabrina, M. Tasinkevych, S. Ahmed, A. M. Brooks, M. Olvera de la Cruz, T. E. Mallouk, K. J. M. Bishop, Shape-directed microspinners powered by ultrasound. *ACS Nano* **12**, 2939–2947 (2018).
48. B. W. Drinkwater, R. S. Trask, Ultrasonic assembly of anisotropic short fibre reinforced composites. *Ultrasonics* **54**, 1015–1019 (2014).
49. P. Wadsworth, I. Nelson, D. L. Porter, B. Raeymaekers, S. E. Naleway, Manufacturing bioinspired flexible materials using ultrasound directed self-assembly and 3D printing. *Mater. Design* **185**, 108243 (2020).
50. R. R. Collino, T. R. Ray, R. C. Fleming, J. D. Cornell, B. G. Compton, M. R. Begley, Deposition of ordered two-phase materials using microfluidic print nozzles with acoustic focusing. *Extreme Mech. Lett.* **8**, 96–106 (2016).
51. M. D. Haslam, B. Raeymaekers, Aligning carbon nanotubes using bulk acoustic waves to reinforce polymer composites. *Compos. Part B Eng.* **60**, 91–97 (2014).
52. Z. Zhang, J. Xu, Y. Pan, 3D-printed polymer composites with acoustically assembled multidimensional filler networks for accelerated heat dissipation. *Compos. B Eng.* **174**, 106991 (2019).
53. S. Oberti, A. Neild, J. Dual, Manipulation of micrometer sized particles within a micromachined fluidic device to form two-dimensional patterns using ultrasound. *J. Acoust. Soc. Am.* **121**, 778–785 (2007).
54. D. J. Collins, C. Devendran, Z. C. Ma, J. W. Ng, A. Neild, Y. Ai, Acoustic tweezers via sub-time-of-flight regime surface acoustic waves. *Sci. Adv.* **2**, e1600089 (2016).
55. D. J. Collins, B. Morahan, J. Garcia-Bustos, C. Doerig, M. Plebanski, A. Neild, Two-dimensional single-cell patterning with one cell per well driven by surface acoustic waves. *Nat. Commun.* **6**, 8686 (2015).
56. J. J. Shi, D. Ahmed, X. Mao, S. C. S. Lin, A. Lawit, T. J. Huang, Acoustic tweezers: Patterning cells and microparticles using standing surface acoustic waves (SSAW). *Lab Chip* **9**, 2890–2895 (2009).
57. A. L. Bernassau, P. Glynne-Jones, F. Gesellchen, M. Riehle, M. Hill, D. R. S. Cumming, Controlling acoustic streaming in an ultrasonic heptagonal tweezers with application to cell manipulation. *Ultrasonics* **54**, 268–274 (2014).
58. F. Gesellchen, A. L. Bernassau, T. Dejardin, D. R. S. Cumming, M. O. Riehle, Cell patterning with a heptagon acoustic tweezer application in neurite guidance. *Lab Chip* **14**, 2266–2275 (2014).
59. Z. Tian, S. Yang, P. H. Huang, Z. Wang, P. Zhang, Y. Gu, H. Bachman, C. Chen, M. Wu, Y. Xie, T. J. Huang, Wave number-spiral acoustic tweezers for dynamic and reconfigurable manipulation of particles and cells. *Sci. Adv.* **5**, eaau6062 (2019).
60. Z. Ma, A. W. Holle, K. Melde, T. Qiu, K. Poeppel, V. M. Kadiri, P. Fischer, Acoustic holographic cell patterning in a biocompatible hydrogel. *Adv. Mater.* **32**, e1904181 (2020).
61. Y. Gu, C. Chen, J. Rufo, C. Shen, Z. Wang, P. H. Huang, H. Fu, P. Zhang, S. Cummer, Z. Tian, T. J. Huang, Acoustofluidic holography for micro- to nanoscale particle manipulation. *ACS Nano* **14**, 14635–14645 (2020).
62. M. Baudoin, J. C. Gerbedoen, A. Riaud, O. B. Matar, N. Smagin, J. L. Thomas, Folding a focalized acoustical vortex on a flat holographic transducer: Miniaturized selective acoustical tweezers. *Sci. Adv.* **5**, eaav1967 (2019).
63. M. Baudoin, J.-L. Thomas, R. A. Sahely, J.-C. Gerbedoen, Z. Gong, A. Sivery, O. B. Matar, N. Smagin, P. Favreau, A. Vlandas, Spatially selective manipulation of cells with single-beam acoustical tweezers. *Nat. Commun.* **11**, 4244 (2020).
64. A. C. Bakenecker, A. von Gladiss, H. Schwenke, A. Behrends, T. Friedrich, K. Lüdtke-Buzug, A. Neumann, J. Barkhausen, F. Wegner, T. M. Buzug, Navigation of a magnetic micro-robot through a cerebral aneurysm phantom with magnetic particle imaging. *Sci. Rep.* **11**, 14082 (2021).
65. G. Go, A. Yoo, K. T. Nguyen, M. Nan, B. A. Darmawan, S. Zheng, B. Kang, C.-S. Kim, D. Bang, S. Lee, K.-P. Kim, S. S. Kang, K. M. Shim, S. E. Kim, S. Bang, D.-H. Kim, J.-O. Park, E. Choi, Multifunctional microrobot with real-time visualization and magnetic resonance imaging for chemoembolization therapy of liver cancer. *Sci. Adv.* **8**, eabq8545 (2022).
66. H. Lee, D.-I. Kim, S.-H. Kwon, S. Park, Magnetically actuated drug delivery helical microrobot with magnetic nanoparticle retrieval ability. *ACS Appl. Mater. Interfaces* **13**, 19633–19647 (2021).
67. G. Go, S.-G. Jeong, A. Yoo, J. Han, B. Kang, S. Kim, K. T. Nguyen, Z. Jin, C.-S. Kim, Y. R. Seo, J. Y. Kang, J. Y. Na, E. K. Song, Y. Jeong, J. K. Seon, J.-O. Park, E. Choi, Human adipose–derived mesenchymal stem cell–based medical microrobot system for knee cartilage regeneration in vivo. *Sci. Robot.* **5**, eaay6626 (2020).
68. B. A. Auld, *Acoustic fields and waves in solids* (John Wiley & Sons Inc., 1973).
69. J. L. Rose, *Ultrasonic waves in solid media* (Cambridge Univ. Press, 1999).
70. L. P. Gor'kov, On the forces acting on a small particle in an acoustical field in an ideal fluid. *Soviet Physics Doklady* **6**, 773 (1962).
71. H. Bruus, Acoustofluidics 7: The acoustic radiation force on small particles. *Lab Chip* **12**, 1014–1021 (2012).
72. O. A. Sapozhnikov, M. R. Bailey, Radiation force of an arbitrary acoustic beam on an elastic sphere in a fluid. *J. Acoust. Soc. Am.* **133**, 661–676 (2013).

Acknowledgments

Funding: We acknowledge the support from the National Institutes of Health (R01GM144417) and the National Science Foundation (CMMI 2243771, CMMI 2340016, CBET 2202688, CBET 2133017, and ECCS 1808931). **Author contributions:** T.L. and Z.T. conceived the idea. T.L. and J.L. designed and manufactured the acoustic vortex devices. L.B. performed acoustic field characterization experiments. T.L. performed contactless acoustic particle manipulation experiments. T.L. performed analytical simulations. J.C., H.B., and B.F. participated in the project discussion. All the authors contributed to the paper writing. Z.T. provided overall guidance and supervised the study. **Competing interests:** The authors declare that they have no competing interests. **Data and materials availability:** All data needed to evaluate the conclusions in the paper are present in the paper and/or the Supplementary Materials.

Submitted 11 November 2023
Accepted 19 April 2024
Published 24 May 2024
10.1126/sciadv.adm7698